Uniformity, Ideality, and Hydrogen Bonds in Transmembrane α-Helices

Sanguk Kim* and Timothy A. Cross*†
*National High Magnetic Field Laboratory (NHMFL), Institute of Molecular Biophysics; and †Department of Chemistry and Biochemistry, Florida State University, Tallahassee, Florida 32310 USA

ABSTRACT Protein environments substantially influence the balance of molecular interactions that generate structural stability. Transmembrane helices exist in the relatively uniform low dielectric interstices of the lipid bilayer, largely devoid of water and with a very hydrophobic distribution of amino acid residues. Here, through an analysis of bacteriorhodopsin crystal structures and the transmembrane helix structure from M2 protein of influenza A, some helices are shown to be exceptionally uniform in hydrogen bond geometry, peptide plane tilt angle, and backbone torsion angles. Evidence from both the x-ray crystal structures and solid-state NMR structure suggests that the intramolecular backbone hydrogen bonds are shorter than their counterparts in water-soluble proteins. Moreover, the geometry is consistent with a dominance of electrostatic versus covalent contributions to these bonds. A comparison of structure as a function of resolution shows that as the structures become better characterized the helices become much more uniform, suggesting that there is a possibility that many more uniform helices will be observed, even among the moderate resolution membrane protein structures that are currently in the Protein Data Bank that do not show such features.

INTRODUCTION

While there has been considerable discussion in the literature about a different balance of molecular interactions that stabilize proteins in a membrane environment, there has been less discussion and evidence for how this balance affects the uniformity of helical structures in this environment. Not only are electrostatic interactions strengthened by the low dielectric of the bilayer interstices, but a greater fraction of these interactions is associated with secondary structural elements, and fewer with tertiary structure. Consequently, the hydrogen bonds stabilizing a helix are strengthened, even though tertiary interactions that might distort helices, while critical for helix-helix packing (Bowie, 2000; Zhou et al., 2000), are less frequent. As a result, the potential exists for observing nearly ideal helical structures in such an environment. Here, we will show through solid-state NMR and x-ray crystallographic structures that such helices exist in a membrane environment.

Helices are the most common secondary structure found in globular proteins, and many analyses have been performed on α-helical structural geometry, packing, and regularity (Chothia et al., 1977; Richmond and Richards, 1978; Barlow and Thornton, 1988). Helices from water-soluble proteins display a considerable spread of ϕ, ψ torsion angles as a result of numerous interactions between the helix and its heterogeneous environment, potentially including the aqueous surroundings, the hydrophobic protein interior, and hydrophilic regions. These interactions are asymmetrically distributed about and along the helical axis. In addition, the asymmetric access of water to a helix can cause considerable helix distortions and bending, because water competes for the intramolecular hydrogen bonds that primarily stabilize these structures (Pauling et al., 1951). Such interactions can lead to both local and global distortions of the helices.

For transmembrane proteins of plasma membranes, helical secondary structure dominates even more than in water-soluble proteins. Furthermore, the environment for such transmembrane helices is more uniform than for water-soluble proteins. Although we often and correctly think of the membrane as a very heterogeneous environment, the bilayer's interior has a uniform low dielectric. Even when considering the interior of large membrane proteins with numerous transmembrane helices, the dielectric is apt to be very low due to the preponderance of hydrophobic residues (Popot and Engelman, 1990). Consequently, it is anticipated that the amide sites in the interstices of lipid bilayers will not only be partnered to form hydrogen bonds, but they will be optimally aligned to minimize exposure of the amide dipole to the low dielectric environment (Xu and Cross, 1999).

Hydrogen-bonding geometry in globular proteins has been characterized by a range of distances and angles (Baker and Hubbard, 1984; Barlow and Thornton, 1988; Jeffrey and Saenger, 1994). According to Baker and Hubbard (1984), the mean O· · ·H distance for the backbone α-helical hydrogen bond is 2.06 Å and the mean O· · ·N distance is 2.99 Å. Hydrogen bonds are known to have both an electrostatic and covalent component. When the C=O· · ·H angle is approximately 120°, covalency is high, when the angle is 160 ± 20°, electrostatic contributions to the energy are high. Rose, Dill, and co-workers' (Stickle et al., 1992) hydrogen bond study of globular proteins shows that the protein α-helical backbone hydrogen bond angle has an average value of 155°, which reflects a dominant electrostatic contribution.

Submitted February 17, 2002, and accepted for publication June 3, 2002.
Address reprint requests to Timothy A. Cross, 1800 E. Paul Dirac Drive, Tallahassee, FL 32306-4005. Tel: 850-644-0917; Fax: 850-644-1366; Email: cross@magnet.fsu.edu.

0006-3495/02/10/2084/12 $2.00

The nonpolar surfaces of these transmembrane helices lead to very weak interactions between helices. Hydrophobic interactions are not present because of the lack of water in the immediate environment, and consequently interactions are relatively nonspecific long-range electrostatic interactions and van der Waals interactions. As a result, some heterogeneity or dynamics between helices is likely, as reported in numerous cysteine cross-linking studies (e.g., Bauer et al., 1999). However, a few specific hydrogen bonds or short-range specific electrostatic interactions, when present, can substantially constrain these helices, diminishing such heterogeneity or dynamics (Zhou et al., 2000).

Here the structure of the transmembrane peptide of M2 protein (M2-TMP) from influenza A virus is analyzed (Wang et al., 2001). The intact protein is 97 amino acid residues and forms an H^+ channel in the viral coat that is activated at low pH. The channel is formed by a tetrameric bundle of α-helices from four monomers (Holsinger and Lamb, 1991; Sakaguchi et al., 1997). M2-TMP is a 25 residue polypeptide that also demonstrates H^+ channel activity (Duff and Ashley, 1992). The helix is highly hydrophobic with only three polar amino acid residues: Ser-31, His-37, and Trp-41, all of which appear to line the channel pore. The solid-state NMR structure is of the closed state in which His-37 is uncharged. This paper also examines the crystal structures of bacteriorhodopsin, which has now reached high resolution standards (five structures in the Protein Data Bank (PDB) at better than 2 Å resolution) (Leucke et al., 1999a, b, 2000; Belrhali et al., 1999). This protein has a seven-helix bundle that binds retinal in the transmembrane region of the bilayer. Two of the helices, A and D, do not have prolines and have diverse helical tilt angles. These helices were also recognized by Leucke et al. (1999a) as being relatively uniform helical structures and are also very hydrophobic, having only four threonines, a tyrosine, and an aspartic acid between the two helices.

A unique observation in solid-state NMR spectroscopy of aligned samples is that the projection of α-helices oriented with respect to the z-axis is imaged in the PISEMA (polarization inversion spin exchange at the magic angle: Wu et al., 1994) spectrum. Such a projection is very closely correlated with the well-known helical wheel projections (Schiffer and Edmunson, 1967). Transmembrane helices show well-defined patterns of 3.6 resonances per turn in PISEMA spectra that correlate ^{15}N-^{1}H dipolar couplings with anisotropic ^{15}N chemical shifts. The size, shape, and position of these patterns in the PISEMA spectra reflect the helical tilt. The rotational orientation of the helix can also be defined (Marassi and Opella, 2000; Wang et al., 2000). The PISA (polar index slant angles) wheel representation not only characterizes the global helical structure, but also describes the peptide plane orientation to high precision and characterizes the hydrogen bond patterns. The resonance frequencies of the ^{15}N-^{1}H dipolar coupling and anisotropic ^{15}N chemical shifts depend on the transmembrane helix orientation to the external magnetic field (B_o), the magnitude and orientations of the principle elements of the ^{15}N chemical shift tensors, and ^{15}N-^{1}H dipolar interaction. In addition to the structural characterization from PISA wheels, the individual restraints from the PISEMA spectrum can be used to refine the helix to a high-resolution structure (Ketchem et al., 1993, 1997; Wang et al., 2001).

To characterize the uniformity of several transmembrane helices a variety of tools will be used from cataloging the hydrogen bond geometry and PISEMA spectral simulations to a new tool we refer to as a Ramachandran-δ diagram. Moreover, these characterizations are applied both to moderate resolution crystal structures of bacteriorhodopsin and published models of M2-TMP to illustrate that helical uniformity is not always apparent in such structures, and therefore their absence in most PDB files of membrane proteins does not necessarily imply their absence in such proteins.

METHODS

PISEMA spectra simulation

To analyze the helical geometry in bacteriorhodopsin, PISEMA spectra were simulated from their PDB coordinates. Average values of the chemical shift tensors (σ_{11} = 31.3, σ_{22} = 55.2, σ_{33} = 201.8 ppm) from experimental data of the transmembrane α-helix, M2-TMP, and a dipolar magnitude value of 10.735 kHz were used for all amino acids (Wang et al., 2000). The values take into account modest local dynamics of the peptide planes. A typical relative orientation (θ) between the σ_{33} chemical shift tensor element and $\nu_{\|}$ of the dipolar tensor equal to 17° was used (Wang et al., 2000; Marassi and Opella, 2000), consistent with previous experimental characterizations (Teng et al., 1992; Oas et al., 1987). It should be noted that in a helix there will be some variation in tensor element magnitudes, for instance in an analysis of 10 sites in M2-TMP RMS deviations from the average values of σ_{11}, σ_{22}, and σ_{33} given are 1.8, 1.6, and 4.4 ppm, respectively (Wang et al., 2001). Furthermore, the θ value for glycine is ~23°, while experimental data suggest that θ typically varies by only ±2° among the other amino acids (Mai et al., 1993). Glycine tensor element magnitudes are typically consistent with the range described above except that σ_{11} values are a few parts per million lower (Lee and Ramamoorthy, 1998). Consequently, experimental PISEMA spectral resonances will be somewhat more scattered due to chemical shift tensor variation than in the spectral simulations shown here. However, the experimental spectra will show less scatter because the experiments directly reflect the native structure, and not the additional noise associated with the crystallographic data and data analysis. How these factors balance out for experimental PISEMA spectra has yet to be seen. All ^{15}N chemical shifts are relative to the resonance for a saturated solution of $^{15}NH_4NO_3$ at 0 ppm.

Peptide plane tilt angle

The peptide plane tilt (δ) is defined by the angle between the peptide plane and the helical axis. Regular peptide helical models were formed by repeating units having the same ϕ, ψ torsion angles. Delta values were characterized as a function of ϕ, ψ torsion angles by generating regular helices incremented in 5° units over the range of ϕ and ψ between −100° and −10°. The helical axis was defined as in Quine (1999). Briefly, for a

series of peptide planes in a helix, a helical axis can be defined by the screw rotation between two adjacent peptide planes.

$$p_{i+1} = U_\theta^u p_i + t$$

where p represents peptide planes and t is a translation vector. The rotation U_θ^u is uniquely determined by an axis direction **u** and an angle θ, where **u** is a unit vector. Using this approach, a helical axis between peptide planes is defined by this unit vector. Finally, the δ angles are calculated from the angle between the helical axis and the peptide plane formed by the N—C_α and N—C bond vectors of the plane.

Analysis of hydrogen bond

Coordinate sets of membrane protein structures were obtained from the PDB. Hydrogen atoms were added to the x-ray crystal structures using the Biopolymer program (Biopolymer, InsightII, version 2000, Biosym/Molecular Simulations, 9685 Scranton Road, San Diego, CA 92121). The main-chain amide hydrogen atoms were placed on the bisector of the angle C—N—C_α, and in the plane defined by C, O, N, assuming a standard N—H bond length of 1.03 Å. The transmembrane helices used for hydrogen bond analysis were initially identified as α-helices using the secondary-structure definition program DSSP (Kabsch and Sander, 1983) and also described in the secondary structure of PDB coordinate files. The hydrogen bond distances were measured from the ith residue carbonyl O to the i + 4 residue amide H. The hydrogen bond distance is defined as the O· · ·H distance rather than O· · ·N (Baker and Hubbard, 1984). The N-H· · ·O and N· · ·O=C angles were also measured.

In the hydrogen bond analysis here, only the distances and angles for i to i + 4 hydrogen bonds have been calculated to characterize the transmembrane helical uniformity, because the helices under consideration are all α-helices.

Structure refinement with orientational restraints

The refined M2 transmembrane peptide structure (Wang et al., 2001) was obtained by a geometrical search using a search algorithm to obtain a minimum of the global penalty function that incorporates all the orienta-

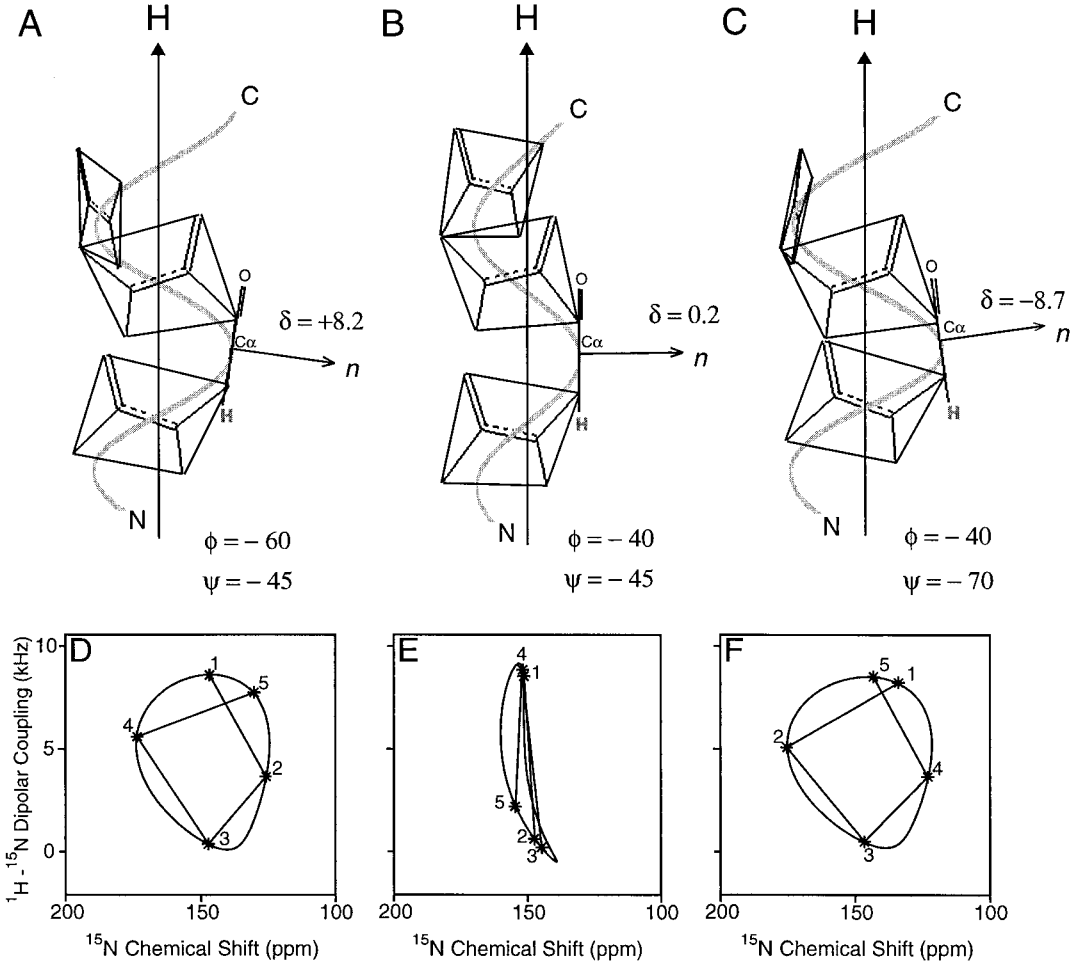

FIGURE 1 The relationship between the peptide plane tilt (δ) and PISA wheel patterns. Three different ϕ, ψ angle combinations were used to generate short regular helical structures. Only four peptide planes are displayed for these structures. The tilt of the peptide plane relative to the helical axis is given by δ, which is calculated as the angle of the peptide plane normal to the helix axis minus 90°. Changing the value of δ by $<10°$ results in a dramatic change in simulated PISA wheels, which represents the simulation of solid-state NMR spectra for a uniformly oriented sample in which the bilayer normal is aligned parallel to the magnetic field direction. Even though all three helical structures (*A–C*) are right-handed helical structures, the PISA wheel pattern changes its handedness from right-handed to left-handed (*D–F*). The tilt angle of the three helices is 38°.

tional restraints, the target hydrogen bond distance in the peptide backbone, and the CHARMM energy function (Brooks et al., 1983; Ketchem et al., 1996). Here the target hydrogen bond distance was varied on different attempts of structure optimization to determine the minimum hydrogen bond energy penalty.

The penalty function used to control the structural refinement is the sum of the structural penalties and the energy, where each structural penalty refers to a particular data type (e.g., ^{15}N chemical shift, ^{15}N-^{1}H dipolar couplings, or hydrogen bond distances):

$$\text{Total Penalty} = \sum_{i=1}^{M} (w_s \cdot \text{Structural Penalty}_i) + w_e \cdot \text{Energy}$$

where M is the number of structural penalties and w is a weighting factor. The individual structural penalties are calculated as,

$$\text{Structural Penalty} = \sum_{j=1}^{N} \frac{1}{2} \left(\frac{\text{Calculated}_j - \text{Observed}_j}{\text{Experimental Error}_j} \right)^2$$

where N is the number of measurements of a specific data type.

The simulated annealing is used to perform the minimization of this penalty function in this high-dimensional configurational space (Metropolis et al., 1953; Kirkpatrick et al., 1983). Modifications to the structure are made by allowing the complete geometry of the polypeptide to vary through modifications of the atomic coordinates and changes in peptide plane orientation (Ketchem et al., 1997). To search the necessary conformational and local structural space, both atom and torsional modifications were used. Random atom moves with a small diffusion parameter of 5×10^{-4} Å in each of three Cartesian axes relaxed the atomic geometry and helped minimize the global penalty. Torsional moves were generated as compensating ψ_i and ϕ_{i+1} moves of equal magnitude and opposite sign (Peticolas and Kurtz, 1980) by a random amount up to $\pm3°$ per step. Because the structural restraints are absolute restraints, i.e., they orient the molecular structure with respect to B_o, it is necessary that the global orientation and local structure be refined. Torsional movements help to adjust the global orientation, while atomic movements allow the local conformational space to be searched. The ratio of attempted atom and torsional moves and other annealing parameters were optimized through numerous refinement attempts (Kim et al., 2001).

The orientational restraints imposed on the structure during refinement are 15 ^{15}N chemical shifts and 15 ^{15}N-^{1}H dipolar couplings from PISEMA experiments. The observed chemical shifts from M2-TMP are compared to calculated values from the molecular coordinates. A change in the orientation of the atomic coordinates leads to a change in the calculated chemical shifts and a resultant change in the penalty. The observed dipolar couplings are also compared to calculated values derived from the atomic coordinates and knowledge of the interaction tensors in the molecular frame of reference. The refinement was carried out in vacuo with the initial coordinates of an ideal α-helical structure with dihedral angles of $\phi = -65$, $\psi = -40$, and having a range of tilt and rotational orientations with respect to the bilayer, spanning the values obtained from the PISA wheels. All calculations were performed by the program TORC (total refinement of constraints) developed for incorporating orientational restraints and the CHARMM energy (Ketchem et al., 1996). The detailed simulated annealing refinement procedure was described earlier (Wang et al., 2001; Kim et al., 2001).

RESULTS

Peptide plane tilt

PISEMA spectra obtained by solid-state NMR spectroscopy from uniformly aligned samples led to the description of PISA wheels. In Fig. 1 the sensitivity of this resonance pattern to the tilt of the peptide planes with respect to the helix axis is shown. Because of the tight packing in an α-helix with 3.6 residues per turn, carbonyl oxygens in the peptide planes are tilted away from the helix axis as shown in Fig. 1 *A*. Indeed, the observation of a PISA wheel is dependent on a significant δ angle. Choosing torsion angles that generate a 0° tilt with respect to the helix axis causes the PISA wheel to collapse, as in Fig. 1 *E*. Furthermore, a tilt of the peptide plane carbonyl toward the helix axis (Fig. 1 *C*) once again results in the observation of a wheel-like pattern, but now the rotational pattern of the resonances is reversed as if the helical sense were reversed, which, of course, is not the case.

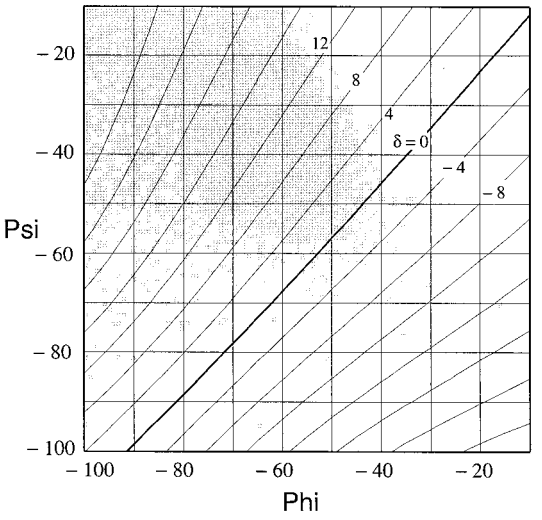

FIGURE 2 Peptide plane tilt angles to the helical axis (δ) are diagramed as a function of ϕ, ψ torsion angles from uniform helical models leading to the development of this Ramachandran-delta diagram. Superimposed on this diagram are ϕ, ψ values from 500 high-resolution ($\leq$1.8 Å resolution) crystal structures (Lovell, Word, Richardson, and Richardson, see http://kinemage.biochem.duke.edu/validation/model.html#rama).

From these models of uniform helices it is clear that the PISA wheels are exquisitely sensitive to this local structure. It is then a logical extension of this observation that there should be a direct correlation between peptide plane tilt and ϕ, ψ torsion angles. In Fig. 2 such a correlation has been achieved by mapping peptide plane tilts characterized from uniform helices of given ϕ, ψ torsion angles. In addition, a region of the map is highlighted illustrating the typical ϕ, ψ space observed in native high-resolution α-helical structures (see legend to Fig. 2). While the regularity of the individual residue ϕ, ψ angles can be used as a measure of helix uniformity, it is difficult to relate this information to a structural picture of helical uniformity. Here we present two new tools for assessing helical uniformity: the PISA wheels and the Ramachandran diagram modified with the peptide plane tilt lines, a Ramachandran-δ diagram. These tools, combined with the measurement of certain distances and angles from coordinates, are used here to evaluate structures

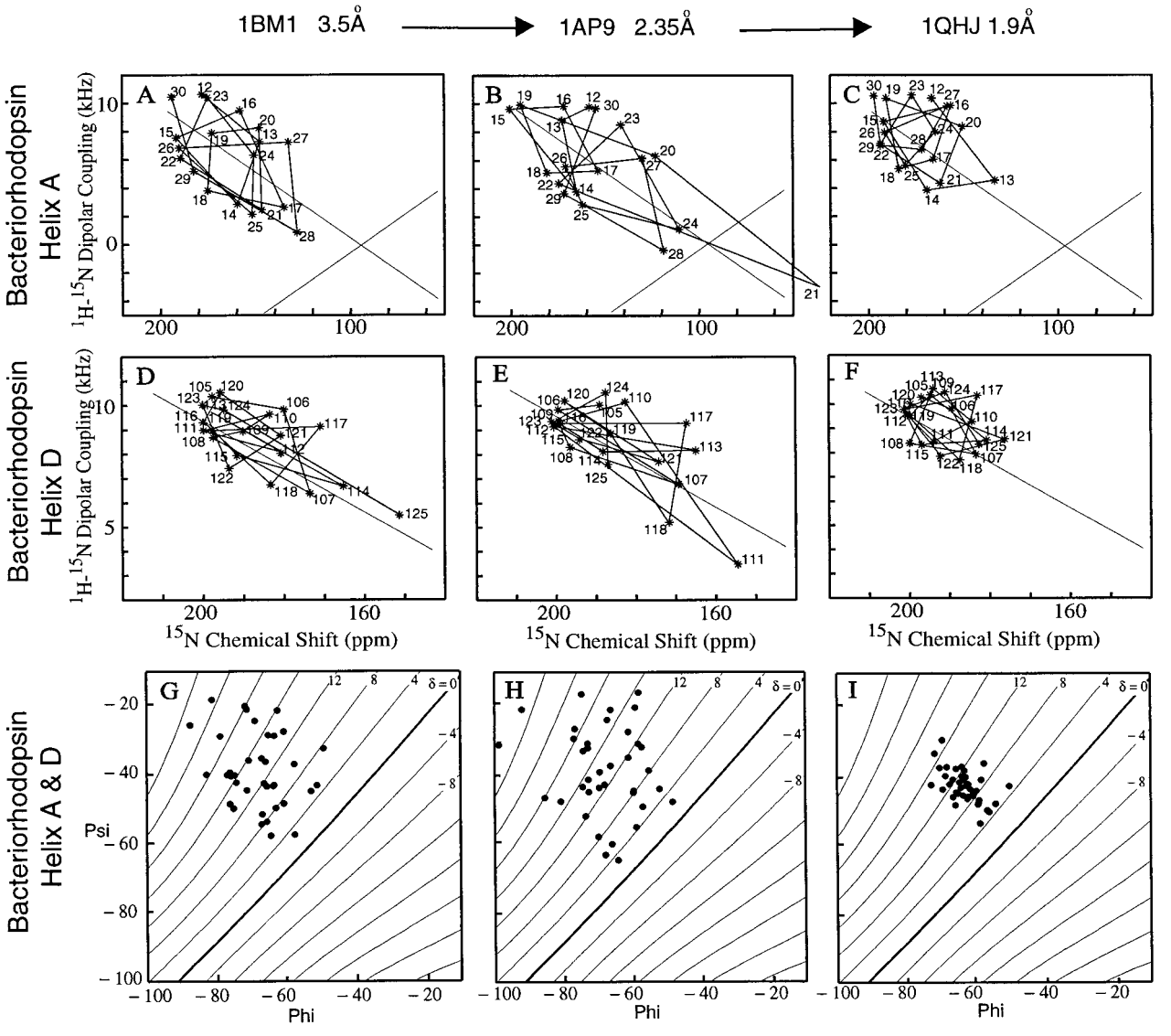

FIGURE 3 PISEMA spectral simulations of bacteriorhodopsin helices A and D. (*A–C*) Helix A (residues 12–30) and (*D–F*) helix D (residues 105–125); (*G–I*) the Ramachandran-delta diagram of helices A and D; (*A, D, G*) 3.5 Å resolution structure, PDB 1BM1 (Sato *et al.,* 1999); (*B, E, H*) 2.35 Å resolution structure, PDB 1AP9 (Pebay-Peyroula *et al.,* 1997). (*C, F, I*) 1.9 Å resolution structure, PDB 1QHJ (Belrhali *et al.,* 1999).

of bacteriorhodopsin and the experimental structure of the M2 transmembrane peptide in addition to structural models of this peptide.

Bacteriorhodopsin

Nine x-ray crystallographic structures from bacteriorhodopsin (PDB ID: 1BM1, 1QM8, 1DZE, 1AP9, 1BRX, 1E0P, 1QHJ, 1F50, 1C3W) have been analyzed to illustrate the uniformity of transmembrane helices and the need for high-resolution structure to observe such uniformity. PISEMA spectra have been simulated for all of these crystal structures having a range of structural resolution, but because the PISA wheel and hydrogen bond analyses show similar patterns for similar resolution structures, only three of these analyses (1BM1, 3.5 Å (Sato et al., 1999); 1AP9, 2.35 Å (Pebay-Peyroula et al., 1997); and 1QHJ, 1.9 Å (Belrhali et al., 1999) resolution) are presented here. Also, from the seven transmembrane helices, two having distinct helical axis tilts are characterized: helix A has a helical axis tilt of approximately 20°, while helix D has a tilt of $<10°$. Although a recognizable PISA wheel is observed in Fig. 3 *A,* the simulations in Fig. 3, *B, D,* and *E* show no evidence of PISA wheels. Indeed, as in Fig. 1 *F,* there is evidence for a reversed PISA wheel pattern in Fig. 3 *B* for residues 12–14 and in Fig. 3 *D* for residues 108– 113. However, from the high-resolution structure, the simulation in Fig. 3, *C* and *F* results in well-defined wheels with ~3.6 resonances per

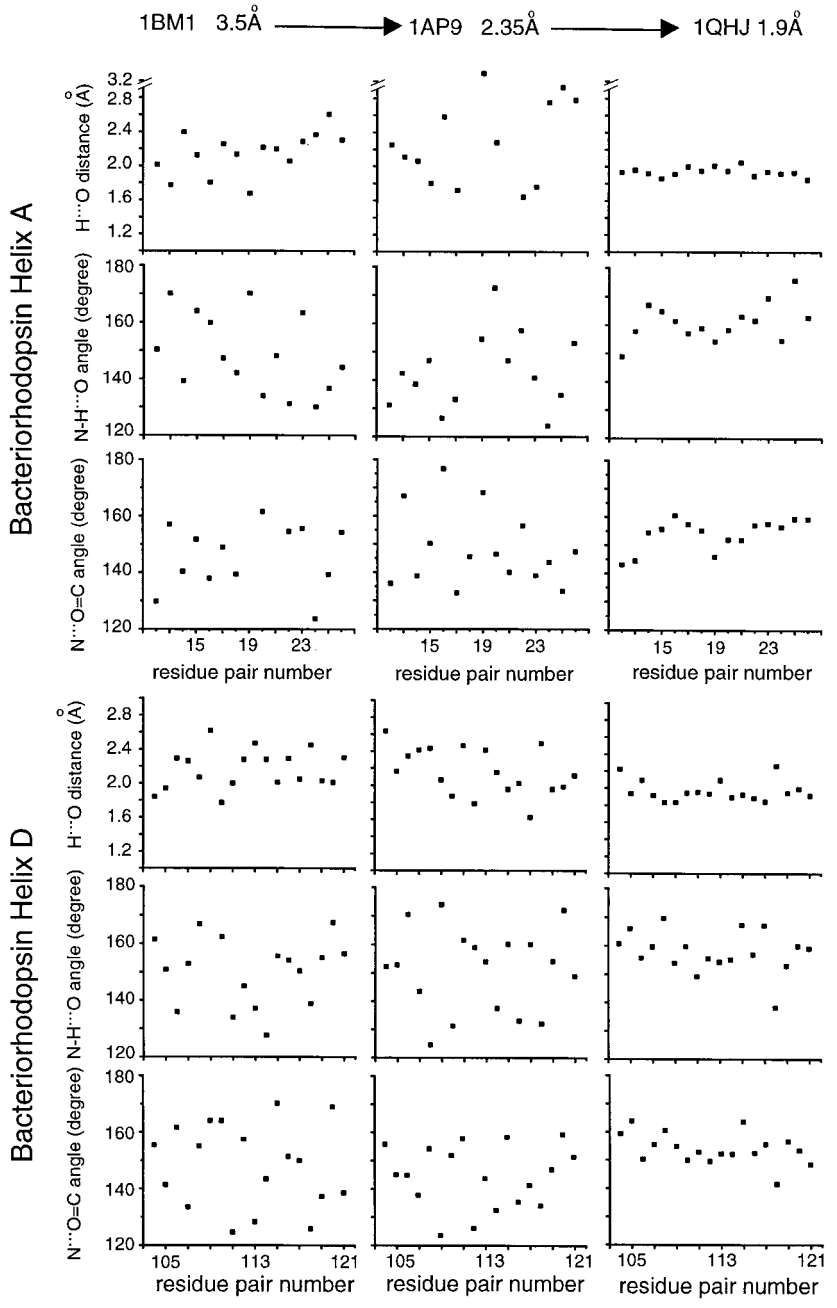

FIGURE 4 Comparison of hydrogen bond distances and angles from bacteriorhodopsin x-ray crystallography structures at different resolution (1.9 Å 1QHJ, 2.35 Å 1AP9, 3.5 Å 1BM1) for helices A and D.

turn. The result in Fig. 3 *F* is especially surprising considering the expanded scale for the helix D spectra and the small tilt angle for this helix.

Along with the improvement in resolution, the distribution of ϕ, ψ torsion angles becomes substantially smaller for these two helices and clustered more closely to the -60, $-45°$ values of an ideal helix (Fig. 3, *G–I*). The range in peptide plane tilt angles is reduced by a factor of two from the 3.5 and 2.35 Å resolution structures to the 1.9 Å resolution structure. This pattern of improved uniformity with experimental resolution is continued in the analysis of hydrogen bond geometry (Fig. 4). The 1BM1 and 1AP9 structures show broken hydrogen bonds and a great range of N—H· · ·O and N· · ·O=C angles. Structure 1QHJ shows a greatly reduced dispersion in hydrogen bond lengths and bond angles. These observations of helical structure regularity, as characterized by PISA wheels, Ramachandran-δ diagrams and peptide plane tilt angles, and uniform hydro-

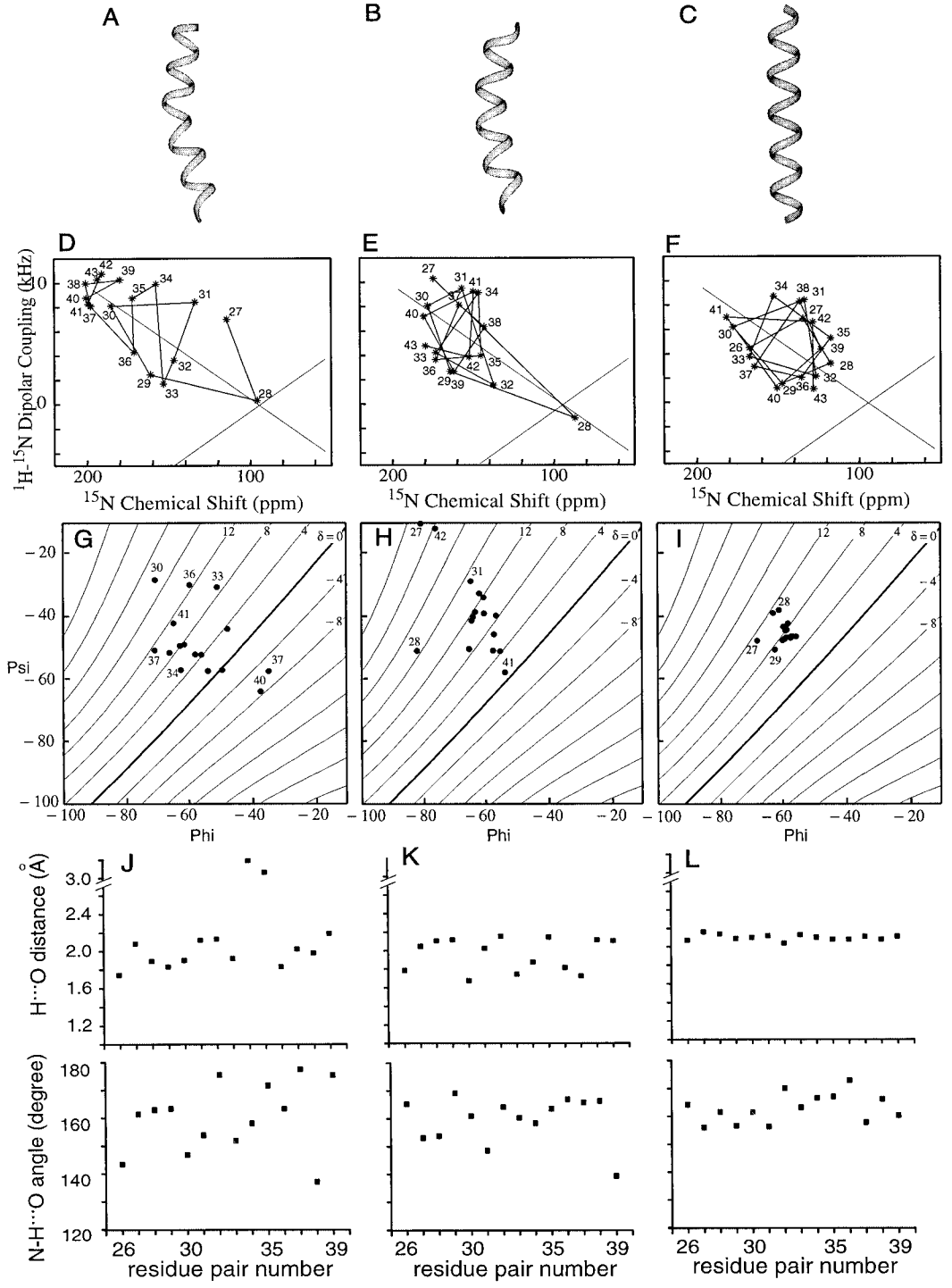

FIGURE 5 Various transmembrane helical model structures of M2-TMP (residues 26–43) and their characterization. (*A*) A calculated structure from a molecular dynamics simulation in a bilayer environment using water/DMPC (Schweighofer and Pohorille, 2000). (*B*) A refined M2-TMP structure based on limited infrared linear dichroism orientational restraints and a coiled coil assumption (Kukol *et al.,* 1999). (*C*) A refined M2-TMP structure from solid-state NMR experimental data (Wang *et al.,* 2001). (*D, E*) Predicted PISA wheels from models *A* and *B*, respectively. (*F*) Solid-state NMR experimental resonance positions from M2-TMP (resonances from residues 31, 34, and 37 are not experimentally observed, but were predicted from the refined structure). (*G–I*) The backbone torsion angles are represented in Ramachandran-delta diagrams. (*J–L*) Hydrogen bond distances and angles measured from the structures in *A–C*. The residue pair number represents the *i*th residue that hydrogen-bonds its carbonyl oxygen to the amide hydrogen of residue $i + 4$. Note that in the M2-TMP refinement (Wang et al., 2001) an H· · ·O constraint of 2.06 Å was used as the target length.

gen bonding geometry were also found in other high-resolution bacteriorhodopsin structures that have a crystallographic resolution better than 2 Å. In fact, among the structures of bacteriorhodopsin with a resolution better than 2.0 Å (1QHJ, 1F50, 1F4Z, 1C8R, and 1C3W) an average of 1.95 Å for the H···O distance is observed based on 716 hydrogen bonds from all seven transmembrane helices in these structures.

Transmembrane helix of M2-protein, M2-TMP

Monomer helices of M2-TMP bundles described in the literature (Schweighofer and Pohorille, 2000; Kukol et al., 1999) are shown in Fig. 5, *A* and *B,* while the recently published structure of this helix in a lipid bilayer environment (Wang et al., 2001) is shown in Fig. 5 *C.* The simulated PISEMA spectra for the models are presented in Fig. 5, *D* and *E,* while a representation of the experimental PISEMA spectra of M2-TMP is in Fig. 5 *F.* The model in Fig. 5 *A* is from a molecular dynamics simulation snapshot and shows both substantial distortions in the helix and obliteration of the PISA wheel. As in the low-resolution structures of bacteriorhodopsin, both left- and right-handed turns in the PISA wheel are observed. Turns at the amino-terminus suggest a tilt of the helical axis $>40°$, while turns at the carboxy-termini suggest helical tilt values of $<10°$. The Ramachandran-δ diagram in Fig. 5 *G* shows a broad distribution of torsion angles and peptide plane tilt angles. These negative values of the peptide plane tilt help to explain the reversed sense of the resonance pattern observed in the PISEMA spectrum. In addition, the hydrogen bond geometry (Fig. 5 *J*) indicates broken bonds (H···O distance >3.0 Å) in this transmembrane helix between residues 34 and 37 and 35 and 38. Although some scatter in the ϕ, ψ angles and hydrogen bond geometry is anticipated considering that this is a molecular dynamics snapshot structure, the extent of helix kinking and distortion is not consistent with the experimental structure or the native environment.

The helix in Fig. 5 *B* is derived from a coiled coil model of M2-TMP based, in part, on linear dichroism IR data. The distance between adjacent helices is maintained at a constant 10 Å separation along the length of the helical axis. Despite the appearance that the helical tilt varies from one end of the helix to the other, it does not, as reflected in a constant center of mass for the PISA wheel (Fig. 5 *E*). This wheel is substantially distorted in only the first couple of residues. Likewise, the Ramachandran-δ diagram shows a couple of outliers with the remaining residues well clustered about -60, $-45°$ with a dispersion in peptide plane tilt angles of $8 \pm 7°$. This coiled coil structure does show an anticipated oscillation in H···O length as hydrogen bonds are compressed on the inside of the coil and stretched on the outside, but otherwise the variation in angle and distance is modest.

The representation of the experimental data (Fig. 5 *F*) shows a very well-defined PISA wheel, somewhat surprising in light of the fact that it reflects more sources of scatter than in the PISEMA simulations. An initial experimental structure of this peptide has been refined using the CHARMM force field and the experimental restraints. The resulting structure has a narrow range of ϕ, ψ torsion angles and peptide plane tilt angles ($8 \pm 3°$) (Fig. 5 *I*). The hydrogen bond geometry is uniform in both distance and angle (Fig. 5 *L*).

In light of the short hydrogen bond lengths that have been observed in the high-resolution bacteriorhodopsin structures, the M2-TMP structure has been refined here while incrementing the target hydrogen bond (N···O and H···O) distances by 0.02 Å. The CHARMM empirical force field was used for the stereochemical constraints. The force field may influence the structural detail, including hydrogen bonds, especially through the nonbonding interactions (Arora and Jayaram, 1997). To avoid overwhelming the stereochemical term of the total penalty function, different weighting factors between the empirical function and the experimental restraints including the hydrogen bond distances were used. The hydrogen bond residuals show a minimum independent of the weighting factor at a hydrogen bond H···O distance of 2.00 Å in Fig. 6 *A.* Fig. 6 *B* shows a contour map minimum at 2.00 Å for the H···O distance and 2.97 Å for the N···O distance.

DISCUSSION

It has long been assumed that electrostatic interactions would be more dominant in the hydrophobic interstices of lipid bilayers because of the low dielectric of this environment. Consequently, the balance of molecular interactions that stabilize water-soluble proteins will be very different than those for membrane proteins. Indeed, it has been anticipated that hydrogen bonds would be very stable in such an environment not only because of the low dielectric, but also because of the scarcity of water. Water competes for hydrogen bonds, thereby destabilizing these bonds. Here, it is shown that the hydrogen bonds in M2-TMP are significantly shorter than the typical α-helical hydrogen bonds in water-soluble proteins. This result appears to be confirmed by the short hydrogen bonds observed in the highest-resolution membrane protein crystal structures. In globular protein structures H···O distances average 2.06 Å (from 577 hydrogen bonds; Baker and Hubbard, 1984), and therefore the distances from bacteriorhodopsin and M2-TMP are shorter by nearly 0.1 Å, thereby shortening an average transmembrane helix by nearly 0.5 Å. Furthermore, in these structures the average backbone hydrogen bond N···O=C angle appears to be $155° \pm 10°$, typical of hydrogen bonds dominated by electrostatic interactions. If covalency increased in the membrane environment, the H···O=C angle (similar to N···O=C) should shift toward 120° because of

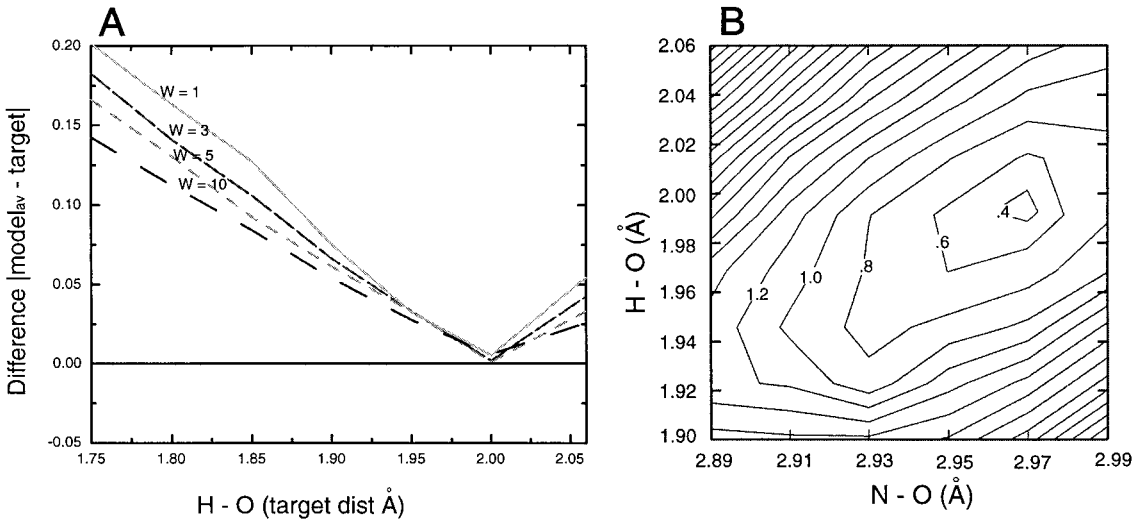

FIGURE 6 (*A*) The penalty value for hydrogen bonds in refining the M2-TMP structure is shown as a function of the target hydrogen bond distances. The penalty for hydrogen bonds is expressed as $E_{\text{hbond}}=w\ \Sigma\ (d_{\text{model}}- d_{\text{target}})$ in the penalty calculation, where w is a weighting factor that balances the empirical versus experimental terms. (*B*) The penalty for the hydrogen bond energy (E_{hbond}) is shown as contours for the M2-TMP backbone structure. The N· · ·O and H· · ·O target distances were searched to find the optimum for the E_{hbond} function.

the sp^2 hybridization of the oxygen. Therefore, the shorter bonds appear to be the result of increased electrostatic interactions.

Although it was tempting for Brunger, Arkin, and coworkers (Kukol et al., 1999) to consider the tetrameric bundle of M2-TMP as a coiled coil, this results in a significant variation in hydrogen bond length. The coiled coil geometry stretches the hydrogen bonds on the exterior of the complex where the dielectric is lowest and compresses the hydrogen bond lengths on the interior of the tetramer that forms a pore, which is more hydrophilic. The increased significance of the hydrogen bonds in the membrane environment results in a tendency toward uniformity of the hydrogen bond geometry. This uniformity is observed not only in M2-TMP, but also in bacteriorhodopsin. The ϕ, ψ conformational space occupied by M2-TMP and helices A and D of bacteriorhodopsin is very small compared to the space occupied by high-resolution x-ray structures of α-helices in water-soluble proteins.

While the uniform low dielectric of the membrane environment is one factor leading to helical uniformity, there are other important contributors. The lack of water that destabilizes intramolecular hydrogen bonds and leads to the catalysis of hydrogen bond exchange (Arumugam et al., 1996; Xu and Cross, 1999) is certainly another factor. In addition, the amino acid composition of transmembrane helices greatly minimizes the potential for substantial tertiary interactions (Bywater et al., 2001). All of these factors are in sharp contrast to the helices in water-soluble proteins.

Structural improvement simply suggests better definition of coordinates, i.e., a reduction in coordinate error bars; it does not necessarily mean a trend toward uniformity of the molecular structure. What has been shown here with only a few examples is that the trajectory from moderate to high-resolution structures can lead to very uniform transmembrane helical structures. Even now it is not clear how uniform the native helices are in bacteriorhodopsin. Will the torsion angles of the structure in a native membrane environment be even more tightly clustered as they are in the solid-state NMR structure of M2-TMP?

The observation of a few uniform helices does not imply that all transmembrane helices are so uniform, but it does suggest that in the absence of other external forces the tendency will be to form helices that are more uniform than in an aqueous environment by the criteria we have described here. Even in the presence of significant external forces such as the binding of a ligand in the hydrophobic interstices of the lipid bilayer, portions of the helices may be quite regular. Fig. 7 shows the PISEMA spectral simulation for all of the transmembrane helices in the 1.9 Å resolution bacteriorhodopsin structure. Although helices A and D, as shown earlier, form more uniform PISA wheels, the resonance predictions for the other helices are tightly clustered in comparison to many of the simulations in Fig. 3 from lower-resolution structures. Whether the imperfections in the PISA wheels in Fig. 7 reflect helix distortions in the native structure or errors in the crystallographic data and data analysis from the 1.9 Å structure remains to be determined.

Although a number of 3 Å resolution membrane protein structures have recently been solved, it is unlikely that the native proteins have broken hydrogen bonds or even peptide plane tilts that vary over a wide range and torsion angles spread over as broad a range as that observed in water-

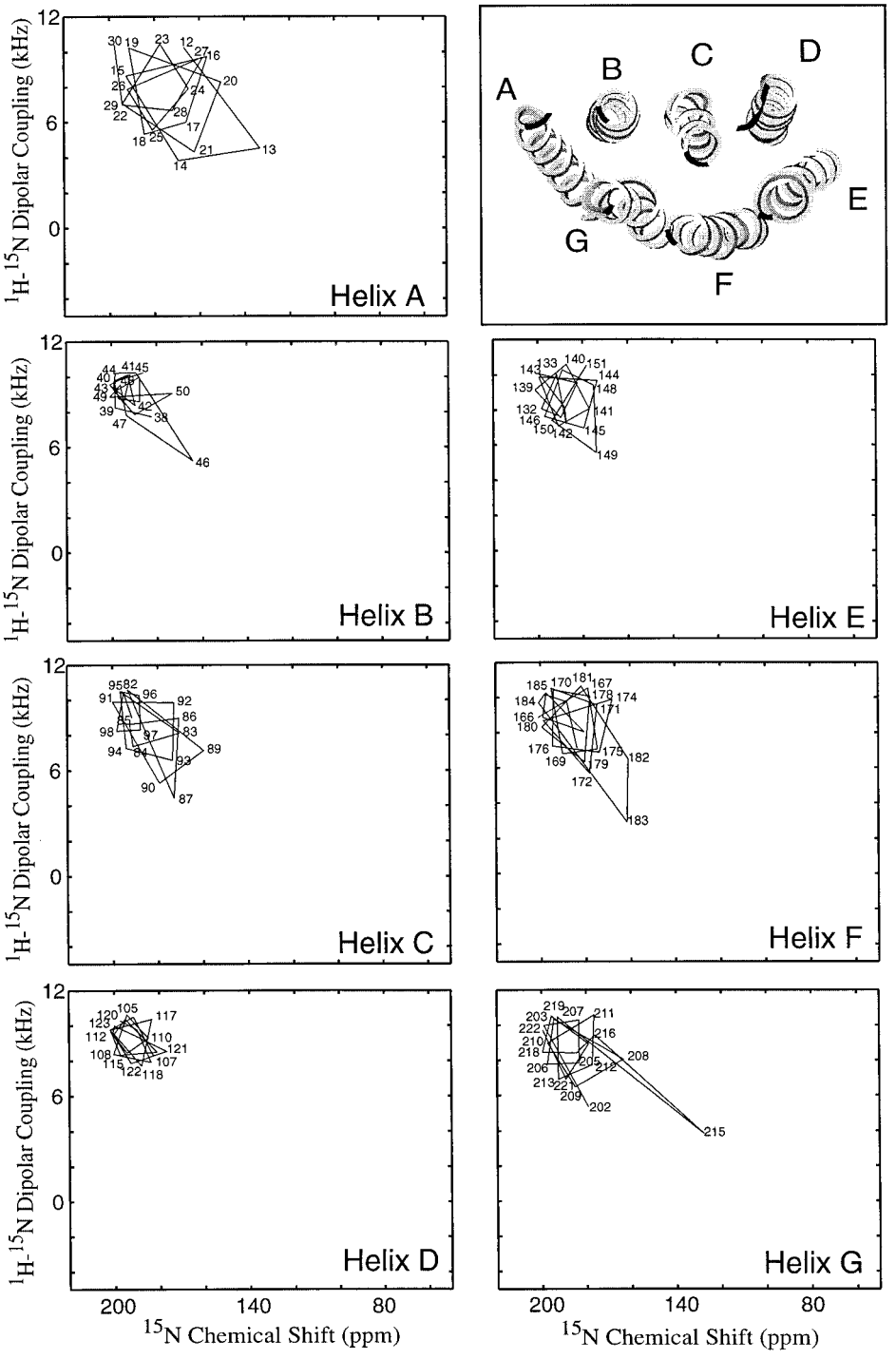

FIGURE 7 PISEMA spectral simulations for all of the transmembrane helices in the 1.9 Å bacteriorhodopsin structure. (*A*) Helix A (residue 12–30); (*B*) helix B (residue 38–60); (*C*) helix C (residue 82– 100); (*D*) helix D (residue 105–125); (*E*) helix E (residue 131–151); (*F*) helix F (residue 166–190); and (*G*) helix G (residue 202–222). Helices A and D duplicate those in Fig. 3. The additional helices show somewhat less uniformity, but the resonances are tightly clustered and the position of the PISA wheels are readily recognized in most of these helices. The small tilt angle for most of these helices further complicates the observation of PISA wheels.

soluble α-helical structures. It may be possible to take advantage of the knowledge expressed here to generate substantially improved structural models based on modest resolution crystal structures. Moreover, in light of the PISEMA spectral simulations from the high-resolution bacteriorhodopsin structures, it can be anticipated that PISA

wheels will be observable for many transmembrane α-helices, and even where helices appear to be distorted and nonuniform in moderate-resolution structures we may expect to see many uniform helices when high-resolution structures are available.

The authors thank Jane Richardson for helpful suggestions.

This work was primarily supported by the National Science Foundation Great DMB 9986036 (to T.A.C.), and the work was largely performed at the National High Magnetic Field Laboratory supported by the National Science Foundation through Cooperative Agreement DMR-0084173 and the State of Florida.

REFERENCES

Arora, N., and B. Jayaram. 1997. Strength of hydrogen bonds in α-helices. *J. Comput. Chem.* 18:1245–1252.

Arumugam, S., S. Pascal, C. L. North, W. Hu, K.-C. Lee, M. Cotton, R. R. Ketchem, F. Xu, M. Brenneman, F. Kovacs, F. Tian, A. Wang, S. Huo, and T. A. Cross. 1996. Conformational trapping in a membrane environment: a regulatory mechanism for protein activity? *Proc. Natl. Acad. Sci. U.S.A.* 93:5872–5876.

Baker, E. N., and R. E. Hubbard. 1984. Hydrogen bonding in globular proteins. *Prog. Biophys. Mol. Biol.* 44:97–179.

Barlow, D. J., and J. M. Thornton. 1988. Helix geometry in Proteins. *J. Mol. Biol.* 201:601–619.

Bauer, C. M., L. H. Pinto, T. A. Cross, and R. A. Lamb. 1999. The influenza virus M2 ion channel protein: probing the structure of the transmembrane domain in intact cells by using engineered disulfide cross-linking. *Virology,* 254:196–209.

Belrhali, H., P. Nollert, A. Royant, C. Menzel, J. P. Rosenbusch, E. M. Landau, and E. Pebay-Peyroula. 1999. Protein, lipid and water organization in Bacteriorhodopsin: a molecular view of the purple membrane at 1.9 angstroms resolution. *Structure (Lond.).* 7:909–917.

Bowie, J. U. 2000. Understanding membrane protein structure by design. *Nat. Struct. Biol.* 7:91–94.

Brooks, B. R., R. E. Bruccoleri, B. D., Olafson, D. J., States, S. Swaminathan, and M. Karplus. 1983. CHARMM: a program for macromolecular energy, minimization and dynamics calculations. *J. Comput. Chem.* 4:187–217.

Bywater, R. P., D. Thomas, and G. Vriend. 2001. A sequence and structural study of transmembrane helices. *J. Comput. Aid. Mol. Des.* 15:533–552.

Chothia, C., M. Levitt, and D. Richardson. 1977. Structure of proteins—packing of alpha-helices and pleated sheets. *Proc. Natl. Acad. Sci. U.S.A.* 74:4130–4134.

Duff, K. C., and R. H. Ashley. 1992. The transmembrane domain of influenza A M2 protein forms amantadine-sensitive proton channels in planar lipid bilayers. *Virology.* 190:485–489.

Holsinger, L. J. and R. A. Lamb. 1991. Influenza virus M2 integral membrane protein is a homotetramer stabilized by formation of disulfide bonds. *Virology.* 183:32–43.

Jeffrey, G. A., and W. Saenger, 1994. Hydrogen Bonding in Biological Structures. Springer-Verlag, Berlin, Heidelberg.

Kabsch, W., and C. Sander. 1983. Dictionary of protein secondary structure: pattern recognition of hydrogen-bonded and geometrical features. *Biopolymers.* 22:2577–2637.

Ketchem, R. R., W. Hu, and T. A. Cross. 1993. High resolution conformation of Gramicidin A in a lipid bilayer by solid-state NMR. *Science.* 261:1457–1460.

Ketchem, R. R., B. Roux, and T. A. Cross. 1996. Computational refinement through solid state NMR and energy constraints of a membrane bound polypeptide. *In* Membrane Structure and Dynamics. K. M. Merz and B. Roux, editors. Birkhauser, Boston. 299–322.

Ketchem, R. R., B. Roux, and T. A. Cross. 1997. High-resolution polypeptide structure in a lamellar phase lipid environment from solid-state NMR derived orientational constraints. *Structure.* 5:1655–1669.

Kim, S., J. R. Quine, and T. A. Cross. 2001. Complete cross-validation and R-factor calculation of a solid-state NMR derived structure. *J. Am. Chem. Soc.* 123:7292–7298.

Kirkpatrick, S., C. D. Gelatt, Jr., and M. P. Vecchi. 1983. Optimization by simulated annealing. *Science.* 220:671–680.

Kukol, A., P. D., Adams, L. M. Rice, A. T. Brunger, and I. T. and Arkin. 1999. Experimental based orientational refinement of membrane protein models: a structure for the influenza A M2 H^+ channel. *J. Mol. Biol.* 286:951–962.

Lee, U. K. and A. Ramamoorthy. 1998. A simple one-dimensional solid-state NMR method to characterize the nuclear spin interaction tensors associated with the peptide bond. *J. Magn. Reson.* 133:204–206.

Luecke, H., B. Schobert, H. T. Richter, J.-P. Cartailler, and J. K. Lanyi. 1999a. Structure of bacteriorhodopsin at 1.55 Å resolution. *J. Mol. Biol.* 291:899–911.

Luecke, H., B. Schobert, H. T. Richter, J.-P. Cartailler, and J. K. Lanyi. 1999b. Structural changes in bacteriorhodopsin during ion transport at 2 Å resolution. *Science.* 286:255–260.

Luecke, H., B. Schobert, H. T. Richter, J.-P. Cartailler, H.-T. Richter, A. Rosengarth, R. Needleman, and J. K. Lanyi. 2000. Coupling photoisomerization of retinal to directional transport in bacteriorhodopsin. *J. Mol. Biol.* 300:1237–1255.

Mai, W., W. Hu, C. Wang, and T. A. Cross. 1993. Three dimensional structural constraints in the form of orientational constraints from chemical shift anisotropy: The polypeptide backbone of gramicidin A in a lipid bilayer. *Protein Sci.* 2:532–542.

Marassi, F. M. and S. J. Opella. 2000. A solid-state NMR index of helical protein structure and topology. *J. Magn. Reson.* 144:150–155.

Metropolis, N., A. W. Rosenbluth, M. N. Rosenbluth, A. H. Teller, and E. Teller, 1953. Equation of state calculations by fast computing machines. *J. Phys. Chem.* 21:1087–1092.

Oas, T. G., C. J. Hartzell, F. W. Dahlqust, and G. P. Drobny. 1987. The carbonyl ^{13}C chemical shift tensors of 5 peptides determined from ^{15}N dipole-coupled chemical-shift powder patterns. *J. Am. Chem. Soc.* 109: 5956–5962.

Pauling, L., R. B. Corey, and H. R. Branson. 1951. The structure of proteins: two hydrogen-bonded helical configurations of the polypeptide chain. *Proc. Natl. Acad. Sci. U.S.A.* 37:205–211.

Pebay-Peyroula, E., G. Rummel, J. P. Rosenbusch, and E. M. Landau. 1997. X-ray structure of bacteriorhodopsin at 2.5 angstroms from microcrystals grown in lipidic cubic phases. *Science.* 277:1676–1681.

Peticolas, W. L., and B. Kurtz. 1980. Transformation of the ϕ-ψ plot for proteins to a new representation with local helicity and peptide torsion angles as variables. *Biopolymers.* 19:1153–1166.

Popot, J.-L. and D. M. Engelman. 1990. Membrane protein folding and oligomerization: the two-stage model. *Biochemistry.* 29:4037–4041.

Quine, J. R. 1999. Helix parameters and protein structure using quaternions. *J. Mol. Struct. (Theochem).* 460:53–66.

Richmond, T. J. and F. M. Richards. 1978. Packing of alpha-helices: geometrical constraints and contact areas. *J. Mol. Biol.* 119:537–555.

Sakaguchi, T., Q. Tu, L. H. Pinto, and R. A. Lamb. 1997. The active oligomeric state of the minimalistic influenza A virus M2 ion channel is a tetramer. *Proc. Natl. Acad. Sci. U.S.A.* 94:5000–5005.

Sato, H., K. Takeda, K. Tani, T. Hino, T. Okada, M. Nakasako, N. Kamiya, and T. Kouyama. 1999. Specific lipid-protein interactions in a novel honeycomb lattice structure of bacteriorhodopsin. *Acta Crystallogr. D.* 55:1251–1256.

Schiffer, M. and A. B. Edmunson. 1967. Use of helical wheels to represent the structures of proteins and to identify segments with helical potential. *Biophys. J.* 7:125–135.

Schweighofer, K. J. and A. Pohorille. 2000. Computer simulation of ion channel gating: the M2 channel on influenza A virus in a lipid bilayer. *Biophys. J.* 78:150–163.

Stickle, D. F., L. G. Presta, K. A. Dill, and G. D. Rose. 1992. Hydrogen bonding in globular proteins. *J. Mol. Biol.* 226:1143–1159.

Teng, Q., M. Iqbal, and T. A. Cross, 1992. Determination of the ^{13}C chemical shift and ^{14}N electric field gradient tensor orientations with respect to the molecular frame in a polypeptide. *J. Am. Chem. Soc.* 114:5312–5321.

Wang, J., J. Denny, C. Tian, S. Kim, Y. Mo, F. Kovacs, Z. Song, K. Nishimura, Z. Gan, R. Fu, J. R. Quine, and T. A. Cross. 2000. Imaging membrane protein helical wheels. *J. Magn. Reson.* 144:162–167.

Wang, J., S. Kim, F. Kovacs, and T. A. Cross. 2001. Structure of the transmembrane region of the M2 protein H^+ channel. *Protein Sci.* 10:2241–2250.

Wu, C. H., A. Ramamoorthy, and S. J. Opella. 1994. High-resolution heteronuclear dipolar solid-state NMR-spectroscopy. *J. Magn. Reson.* 109:270–272.

Xu, F. and T. A. Cross. 1999. Water: foldase activity in catalyzing polypeptide conformational rearrangements. *Proc. Natl. Acad. Sci. U.S.A.* 96:9057–9061.

Zhou, F. X., M. J. Cocco, W. P. Russ, A. T. Brunger, and D. M. Engelman. 2000. Interhelical hydrogen bonding drives strong interactions in membrane proteins. *Nat. Struct. Biol.* 7:154–160.